Two novel resistance-capacitance network models to predict the dynamic thermal behavior of active pipe-embedded structures in buildings

Marcos Hongn, Facundo Bre, Marcelo Valdez, Silvana Flores Larsen

PII: S2352-7102(21)01679-X

DOI: https://doi.org/10.1016/j.jobe.2021.103821

Reference: JOBE 103821

To appear in: *Journal of Building Engineering*

Received Date: 4 October 2021

Revised Date: 22 November 2021

Accepted Date: 3 December 2021

Please cite this article as: M. Hongn, F. Bre, M. Valdez, S.F. Larsen, Two novel resistance-capacitance network models to predict the dynamic thermal behavior of active pipe-embedded structures in buildings, *Journal of Building Engineering* (2022), doi: https://doi.org/10.1016/j.jobe.2021.103821.

Two novel resistance-capacitance network models to predict the dynamic thermal behavior of active pipe-embedded structures in buildings

Marcos Hongn[a,b,*], Facundo Bre[c], Marcelo Valdez[a,b], Silvana Flores Larsen[a,b]

[a] *INENCO - Instituto de Investigaciones en Energía No Convencional, CONICET, Av. Bolivia 5150, Salta, Argentina*
[b] *Universidad Nacional de Salta, Av. Bolivia 5150, Salta Argentina*
[c] *Centro de Investigación de Métodos Computacionales (CIMEC), UNL, CONICET, Predio "Dr. Alberto Cassano", Colectora Ruta Nacional 168 s/n, 3000, Santa Fe, Argentina*

Abstract

Active pipe-embedded structures (APES) are promising low-energy systems for reducing cooling and heating loads in buildings. These structures are usually multilayered, having a main concrete layer where pipes are located. Simplified heat transfer models of these systems are often required for building energy performance simulations. The majority of the simplified models available in the literature show limitations to capture accurately the dynamic thermal behavior of these systems, especially when they have large thermal mass. The goal of the present effort is to introduce two new Resistance-Capacitance (RC) network models, the Delta and the Umbrella, for the main concrete layer of a prototypical APES system. The parameters of the models are obtained through a genetic algorithm, which is dynamically coupled with the models. This algorithm minimizes the error between the RC networks and a baseline dataset that was generated through a frequency-domain finite-difference (FDFD) model of an APES system. To assess the performance of the proposed models, they are compared with two others from the literature for three different thicknesses of the main layer. The results show that the Delta RC network has, in general, similar performance to the literature models. The overall nRMSE (normalized root mean square error) values for these models is between 6% and 10%. They are able to predict accurately the thermal response of the system to some of the boundary conditions analyzed, but show limitations for massive concrete layers under high frequency thermal fluctuations. The Umbrella RC network, on the other hand, was shown to have remarkable accuracy at higher frequencies than the other models, even for the massive structures. The overall nRMSE value for this model was of 3%.

Keywords: Active pipe-embedded structure, Simplified thermal model, RC network, Thermal frequency response, Calibration, Genetic algorithm

1. Introduction

In the last decades, there has been much concern about energy consumption and greenhouse gas emissions. According to the International Energy Agency (IEA) [1], the energy consumption in residential and non-residential buildings represents 25% of the global energy usage, while electricity consumption in operating buildings accounts for nearly 55% of the global electricity consumption. In addition, the carbon emissions associated with building operations have increased to their highest level yet at around 10 $GtCO_2$, which means

*Corresponding author
Email address: mhongn@unsa.edu.ar (Marcos Hongn)

28% of total global energy-related CO_2 emissions. This fact shows that there is great potential for energy use reduction in the building sector alone. The efforts in this area are already in progress. In September of 2020, the Global Alliance for Buildings and Construction (GlobalABC) issued a call to include building renovation and upgrading in COVID-19 recovery plans. This is intended to be a massive renovation wave sponsored by national and local stakeholders through specially tailored support mechanisms. The goal is to make the existing building stock more energy-efficient [2].

The interest in the development of low-energy technologies with applications to the building sector and HVAC systems has grown considerably among the research community [3–5]. These technologies offer reductions in energy consumption, peak energy demand, and energy cost without affecting the desired comfort level conditions of the occupants. Among the alternatives to conventional cooling systems, thermally activated building systems (TABS) have emerged as a promising technology that could deliver user- required thermal comfort and air quality indoor conditions, [6]. The main characteristics of TABS are their high thermal inertia and their large exposed surfaces for heat transfer, which allow significant heat exchange, even with small temperature gradients [7]. In addition to the previous thermal aspects, the selection of the most convenient TABS should take into account other characteristics such as system controllability, short/long term heat storage, suitability of building retrofit and construction cost [8].

The configuration of a given TABS depends on the intended type of operation, the location of the system, and the working fluid employed. Romaní et al. [9] performed a fairly complete review of TABS and identified the fact that there is not a uniformly accepted nomenclature. Therefore, a general typological division was proposed by the authors covering all types of thermally activated solutions (radiant floors, radiant ceilings, hollow core slabs, concrete cores, and embedded pipe envelopes). Some of these configurations may have very high thermal mass due to the presence of heavy-weight material layers. The thermal mass allows these systems to buffer the room temperature fluctuation through the heat management (storage or discharge). When the working fluid employed is water, which flows through pipes deeply embedded into a concrete- made structure, the system is usually referred to as an active pipe-embedded building structure (APES). This term can be applied to horizontal (floor and ceiling) systems, as well as to vertical (wall) systems, which can be used either for heating or cooling indoor spaces [10]. Krajčík et al. [11] compared these configurations from different points of view and concluded that, in certain scenarios, wall systems are preferred to horizontal systems due to their easier installation and/or better energy performance. Also, their performance can be enhanced by adding phase change materials (PCMs).

The APES systems can be coupled to different low-grade energy sources (groundwater, cooling towers, geothermal sources, night radiative cooling, etc.) to reduce the impact of the outdoor climate on the indoor environment, to minimize the heat transfer with the exterior, and to improve the indoor thermal comfort [12].

Due to the large thermal inertia and dynamic nature of APES systems, transient simulations are inevitably required to design and characterize their complex thermal behavior [9, 13]. To evaluate the influence of these elements on the buildings, the global computational model implemented has to take into account the convection process from the working fluid to the slab, the conduction heat transfer through the slab, and also the thermal interaction with surrounding air (external and internal) and with the other building elements, both convective and radiative heat transfer, as appropriate. Numerical models based on the Finite Element Method (FEM) and the Finite Difference Method (FDM) have been shown to accurately describe the heat transfer and the heat storage

capacity of APES [13–15]. In addition, they can be used to solve energy, momentum, and mass conservation differential equations with high temporal and spatial resolutions. Despite their excellent accuracy, one of the main limitations of these approaches is that then require relatively large computational effort. Furthermore, such complex numerical approaches are difficult to integrate into other existing software, such as EnergyPlus^{TM} and TRNSYS, in order to carry out whole building performance simulations. This limitations hinder the application of such high fidelity models for the prediction of the performance of buildings with integrated APES systems, which is crucial for their proper design and optimization. Therefore, the development of simplified but accurate enough models to predict the thermal performance of APEs systems is relevant to the building energy simulation field.

Among the analytical models to predict the APES thermal performance, those that are represented as networks of thermal resistances (R) and heat capacities (C) are very popular [12]. These RC networks are based on the analogy between the electrical conduction and the heat conduction phenomena [16] and their main advantages are that they require low computational effort and can be easily integrated into other software for complete building performance simulations. Often times, the parameters of RC network models are identified in the frequency domain using the results form harmonic heat transfer simulations carried out with more advanced computational models such as FEM, FDM, or Computational Fluid Dynamics (CFD) [17].

One of the pioneer RC network models was proposed and implemented in TRNSYS in [18] to simulate the performance of hydronic concrete core systems. In this model, the network consisted of three resistances and the thermally active element between two walls was idealized as a dummy zone (core layer) that accounts for the water flow in the piping system. Due to its geometrical limitations, the accuracy of this model deteriorates when the period of the temperature fluctuations in the pipe is below 10 h. The same concept of core temperature layer was utilized in [19] to model a pipe-embedded concrete slab through a star RC network configuration. In general, the predictions of the model for steady-state and transient conditions were good enough. However, the accuracy of the model worsens when the temperature fluctuation period is smaller than 2.51 h (6.9×10^{-4} rad/s). Based on the model developed by Koschenz and Dorer [18], Yu et al. [20] proposed a modification to the hydronic radiant module of EnergyPlus^{TM}. This modification included two thermal resistances to account for the heat transfer between the pipe and the virtual core. The model was validated through numerical and experimental studies of the steady state heat transfer on multi-layer floor structures.

A triangular RC-network composed of five resistances and two capacitances, that connect the pipe wall node with the external surfaces nodes (5R2C configuration), was proposed by Zhu et al. [12] to simulate the heat transfer across the width of a pipe-embedded multi-layer structure. The parameters of the model were calibrated through a genetic algorithm (GA) using the frequency responses obtained with a Frequency Domain Finite Difference (FDFD) model as it was done in [21]. The results show that the accuracy of the model decreases for walls with moderate to high thermal mass, and especially over the high-frequency range (10^{-4} to 10^{-3} rad/s). In a related study by Zhu et al. [22], the same RC-network was coupled with an epsilon-NTU model to include the heat transfer phenomenon in the axial direction of the embedded pipes. The obtained semi-dynamical model was validated against CFD simulation results. The model showed reasonable agreement at relatively low frequencies, but was not well suited over high frequency ranges. Li et al. [23] developed and validated an RC thermal network model for pipe-embedded concrete radiant floors. In their approach, the central core was

modeled through a star-type RC configuration and the top and bottom layers with a 2R1C configuration. The parameters of the main layer were also identified through a genetic algorithm (GA) but using the simulation results from Frequency Domain Finite Element (FDFE) model, whose modeling and meshing process is the same as FEM but works in the frequency domain (temperatures and heat fluxes are sinusoidal and expressed in complex form). The results show that the model is able to accurately represent the frequency response of the system in a wide range of frequencies; however, its performance is not as good for medium thickness (100 mm) concrete layers with fast thermal periodic fluctuations.

Two RC network configurations (the star and the triangular configurations) were compared in [24] to predict the heat transfer in thermally activated building components. This study concluded that, although easier to calibrate, the star scheme fails to reproduce the performance of thin slabs. The triangular configuration, on the other hand, was shown more adequate to predict the behavior of ticker slabs (e.g., walls), but the calibration process is more involved due to the large amount of parameters: 15 resistors and 9 capacitors.

Recently, the thermal performance and energy efficiency of a novel PCM-embedded wall system with nocturnal sky radiator for active heat removal was studied by Yan et al. [25]. The heat transfer of the wall was modeled using a 5R2C network as in Zhu et al. [12], whereas for the pipe-encapsulated PCM structure, the 4R2C proposed in a previous work [26] was used. A promising reduction of the cooling loads was observed with the PCM-embedded wall system.

To address the pinpointed limitations of the current simplified models, two novel RC networks are proposed in this article to simulate the dynamical behavior of the main layer of an APES system. The goal of this article is to contribute simple models that can more accurately represent the thermal frequency response characteristics of massive APES over a wider range of thermal fluctuation frequencies, especially on the high end of the spectrum where the current models in the literature fail. Similarly to previous approaches, a two-dimensional FDFD model is used as a reference (baseline) for the calibration and validation of the models. A genetic algorithm is dynamically coupled with the developed models to determine the thermal parameters, resistance and capacitance, that minimize the error relative to the baseline model. Finally, a detailed comparative analysis of the thermal performance of four RC network models (the two developed and two from the literature) is carried out considering three APES systems with 40 mm, 100 mm, and 200 mm concrete layer thicknesses.

2. Methodology

The cross section of an APES system is shown schematically in Fig. 1a. Usually, it is a multi-layer structure composed of a main concrete layer that hosts a single line of embedded pipes and one or more external layers. In the figure, two external layers are represented, one in contact with the outdoor environment (external wall) and the other in contact with the indoor environment (internal wall). In this effort, only the concrete layer is modeled and analyzed.

To simplify the heat transfer model of this structure, the following assumptions are considered:

- heat transfer is two dimensional; hence the heat transfer along the length of the pipes is disregarded,
- between two adjacent embedded pipes there is an adiabatic surface because the water temperature of the pipes is the same (see Fig. 1a),

- the pipe surface temperature is radially uniform and the thermal conductive resistance through pipe wall is negligible,
- the water flow through the pipes is turbulent; therefore, the water temperature is uniform across the section of the pipe.

The governing equation is the dynamic two-dimensional heat equation within the solid part of the APES system, which reads as follows:

$$\rho \; c_p \; \frac{\partial T}{\partial t} = -\frac{\partial \; q''_x}{\partial x} - \frac{\partial q''_y}{\partial y} \tag{1}$$

where $q''_x = -k\frac{\partial T}{\partial x}$ and $q''_y = -k\frac{\partial T}{\partial y}$ are the heat fluxes along the x and y directions, respectively, and ρ, c_p and k are the density ($\mathrm{kgm^{-3}}$), specific heat capacity ($\mathrm{Jkg^{-1}K^{-1}}$) and thermal conductivity ($\mathrm{Wm^{-1}K^{-1}}$), respectively.

2.1. FDFD Baseline Model

The frequency domain finite difference method (FDFD) allows analyzing the frequency thermal responses of the system under different disturbances directly, that is to say, it does not require initial fields and time iterations. It is usually employed to address complex systems in the electromagnetic and acoustic fields. The frequency-domain analysis is generally more convenient than the time-domain analysis for the process of parameter identification of simplified of heat transfer RC networks models. The relation between the frequency-domain and the time-domain is given by the Fourier Transform. In this effort, an FDFD model is implemented to analyze the conductive heat transfer through the APES section shown in Fig. 1a. The numerical scheme is analogous to the one presented by [21], and it is used to generate the frequency responses that constitute the baseline for the calibration and validation of the proposed RC network models.

The frequency responses of the system are obtained by specifying the three main input/output variables, namely, the surface temperatures of the pipe wall and the external and internal faces of the layer in three independent sets of boundary conditions. This approach was shown to be enough to characterize the steady-state response of the system due to all possible combinations of periodic temperature inputs on those surfaces [24], as result of the principle of superposition and the fact that any arbitrary periodic signal can be represented as a Fourier series.

As it will be explained later, in the frequency domain the temperature at any point of the domain is expressed as a zero-mean harmonic disturbance with amplitude $\hat{T}[K]$, phase angle $\phi[rad]$ and frequency $\omega[rad/s]$. The three temperature boundary conditions that are analyzed are summarized as follows:

i. Outside surface temperature with amplitude $\hat{T} = 1$ K and phase $\phi = 0$ rad. All the remaining surfaces with temperature set to 0.
ii. Inside surface temperature with amplitude $\hat{T} = 1$ K and phase $\phi = 0$ rad. All the remaining surfaces with temperature set to 0.
iii. Pipe wall surface temperature with amplitude $\hat{T} = 1$ K and phase $\phi = 0$ rad. All the remaining surfaces with temperature set to 0.

A semi-discrete finite-difference approach is employed to discretize Eq. (1) in the domain *abcd* schematically shown Fig. 1a. Only the first order spatial derivatives of the heat fluxes in Eq. (1) are approximated by a three-point central difference operator. The time derivative of the temperature is not discretized; instead, a periodic solution in complex form is proposed for this variable. The details of the finite-difference equations, obtained according to the methodology presented in [27] are included in Appendix A. The resulting equations can be interpreted as a system of resistors and capacitors connecting the cells as shown in Fig. 1b. Each cell has a central node and the heat transfer between cells occurs at their faces. Each cell is represented by a capacitor (temperature node) and it is connected with the neighboring cells through two thermal resistances in series. Therefore, each cell contains a cross thermal network as shown Fig. 1b.

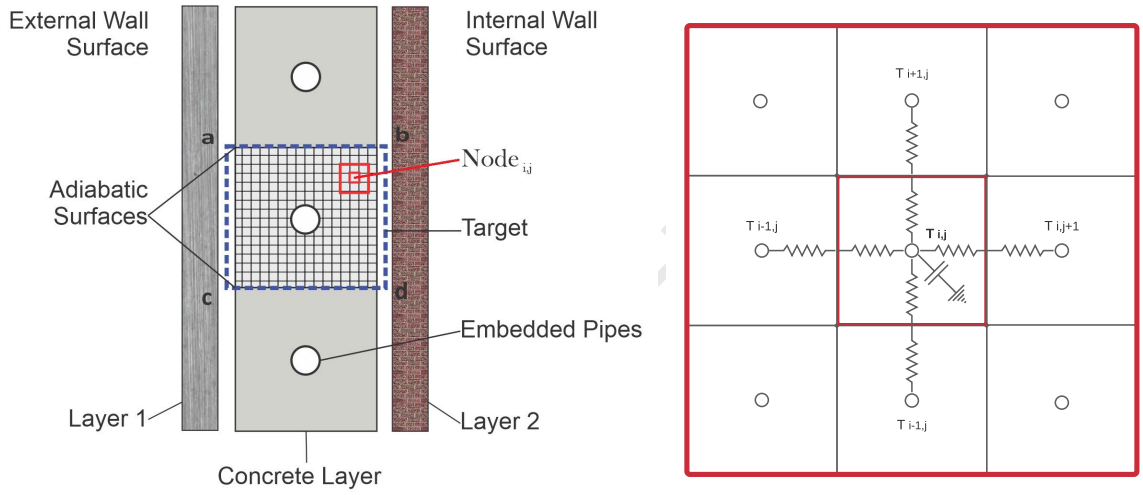

(a) Schematic representation of the cross section and discrete grid model of the APES.

(b) Schematic heat transfer network between node (i, j) and adjacent nodes.

Fig. 1. FDFD representation of APES systems.

As mentioned before, the temperature T_i of a cell i is expressed in complex form as follows:

$$T_i = \hat{T}_i e^{j(\omega t + \phi_i)} = (u_i + j v_i) e^{j\omega t}, \tag{2}$$

where $j = \sqrt{-1}$ is imaginary unit, ω [rad/s] is the frequency, ϕ [rad] is the phase angle, t [s] is the time, u and v are the real and imaginary parts of the complex amplitude $\hat{T}e^{j\phi}$ [K]. Explicitly, the real and imaginary components of T_i, u_i and v_i, respectively, are given by

$$u_i = \hat{T}_i \cos\phi_i, \qquad v_i = \hat{T}_i \sin\phi_i. \tag{3}$$

In terms of u_i and v_i, the temperature amplitude $\hat{T}_i$ and phase angle ϕ_i are given by

$$\hat{T}_i = \sqrt{u_i^2 + v_i^2}, \qquad \phi_i = \arctan\left(\frac{v_i}{u_i}\right) \tag{4}$$

For each cell, the thermal equilibrium equation with the adjacent cells is written in terms of the heat flow balance according to Fig. 1b. For the (i, j) node, the discrete two-dimensional heat balance equation is derived from the Eq. (1) and expressed as follows:

$$dxdy\rho c_p \frac{\partial T_{i,j}}{\partial t} = U_n(T_{i+1,j} - T_{i,j}) + U_e(T_{i,j+1} - T_{i,j}) + U_s(T_{i-1,j} - T_{i,j}) + U_w(T_{i,j-1} - T_{i,j}), \tag{5}$$

where the partial derivative on the left side of the Eq. (5), considering the temperature as complex variable, is calculated as:

$$\frac{\partial T_{i,j}}{\partial t} = j\ \omega\ T_{i,j} \tag{6}$$

Introducing Eqs. (2) and (6) in Eq. (7), the heat equation for the (i, j) node is expressed as frequency function only (due to the suppression of the therm $e^{j\omega t}$). The heat transfer coefficients U (conductances) are calculated according to Eq. (7) as:

$$U_{n;s} = \frac{dx_{i,j}}{\frac{dy_{i,j}}{2k_{i,j}} + \frac{dy_{i,j\pm1}}{2k_{i,j\pm1}}},\ U_{e;w} = \frac{dy_{i,j}}{\frac{dx_{i,j}}{2k_{i,j}} + \frac{dx_{i\pm1,j}}{2k_{i\pm1,j}}}. \tag{7}$$

In Eq. (7), the positive or negative sign in de denominator depends on the relative position of the neighbor node: $(+)$ for north and east, and $(-)$ for south and west. Eq. (5) must be simultaneously solved for all the nodes of the grid. Replacing eq. (2) into (5) yields the frequency domain finite difference equation, whose matrix form for the node (i, j) is given in Eq. (8). Extending this analysis to all nodes yields a $2N_{\text{nodes}} \times 2N_{\text{nodes}}$ non-symmetrical sparse coefficients matrix and a $2N_{\text{nodes}} \times 1$ solution vector that contain the real and imaginary parts of the temperature at each cell.

$$\begin{bmatrix} U_n + U_e + U_s + U_w & -dx\,dy\,\rho\,c_p\,\omega \\ dx\,dy\,\rho\,c_p\,\omega & U_n + U_e + U_s + U_w \end{bmatrix} \begin{bmatrix} u_{i,j} \\ v_{i,j} \end{bmatrix} = \begin{bmatrix} U_n\,u_{i+1,j} + U_e\,u_{i,j+1} + U_s\,u_{i-1,j} + U_w\,u_{i,j-1} \\ U_n\,v_{i+1,j} + U_e\,v_{i,j+1} + U_s\,v_{i-1,j} + U_w\,v_{i,j-1} \end{bmatrix} \tag{8}$$

2.2. Current RC network models

The RC network models are excellent candidates to represent the dynamic performance of APES systems [22]. Comparing heat transfer fluxes at different surfaces, acceptable results have been obtained using *star* and *triangular* RC networks. However, the results reported in the literature show that the accuracy of the predicted frequency responses usually worsens in the range of high frequencies between 10^{-4} and 10^{-3} rad/s (thermal variations with periods between 17.45 h and 1.74 h). Moreover, the dynamic performance of these models decreases when the APES elements are made of materials with high thermal mass.

From the available state-of-art models, two were selected: the Star RC network (Fig. 2a) and the 5R2C network (Fig. 2b). They were computational implemented in this effort in order to compare them with the new models proposed. These models can be used to simulate horizontal (slab) as well as vertical (wall) elements. The 5R2C network can be considered a triangular RC configuration since the connections between the pipe node and the superficial nodes (on the outside and inside surfaces) are direct.

In this work, the focus is only on the main (usually concrete) layer of APES systems, which contains the embedded pipes. The other layers that compose the APES system may be simulated as simple 2R1C thermal networks [23]. The main concrete layer can be modeled as a core layer with external layers, as it is the case of the Star RC network (see Fig. 2a), or as a single layer in the case of the 5R2C network (see Fig. 2b). Indeed, the 5R2C configuration is used to simulate multi-layered systems (three-layer elements), where the whole element is represented by this RC configuration [12].

2.3. New RC network models

In this section, two new RC networks are proposed and derived. The first model is a triangular-based RC network, which we name Delta RC network. The second one is a combined configuration inspired by Star and Delta networks and their corresponding performances, which we name Umbrella RC network.

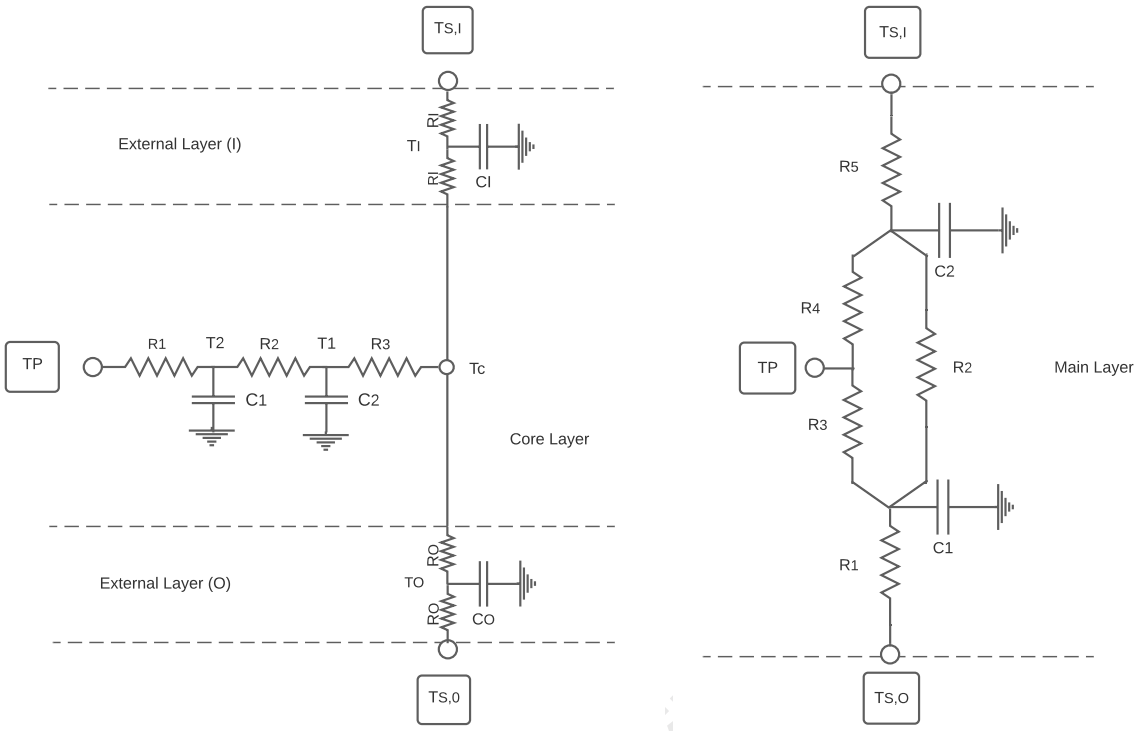

(a) Star RC network [23]

(b) 5R2C RC network [12]

Fig. 2. State-of-art thermal RC networks.

2.3.1. Delta RC network model

Fig. 3 shows the Delta RC network proposed. This configuration represents the thermal behavior of the core layer while the adjacent surfaces of the main concrete layer could be determined as 1R2C thermal networks. This kind of model does not consider a thermal direct connection between the pipe node and the virtual core layer temperature, unlike the star RC models. In Fig. 3, T_P is the temperature of the pipe surface, while $T_{S,O}$ and $T_{S,I}$ are the temperatures of the outside and inside APES surfaces, respectively. These three nodes are considered as temperature inputs in the analysis of simplified RC models. For the delta RC network, the parameters to be determined are: $R_1, R_2, R_3, R_4, R_5, C_1$ and C_2. The parameters R_O, R_I, C_O and C_I can be expressed as functions of the thermal resistances that make up the triangular network (core layer).

Under steady-state conditions (for frequencies ω close to 0 rad/s) the RC network becomes a purely resistive network. This resistive Delta network can be transformed into an equivalent resistive star network, which, in turn, allows expressing the external layer resistances R_O and the internal layer resistances R_I in terms of R_1,...,R_5. Then, the heat capacitances C_O and C_I are calculated as functions of the material properties and resistances R_O and R_I, respectively. To solve the heat transfer problem, the heat balance equation for each node

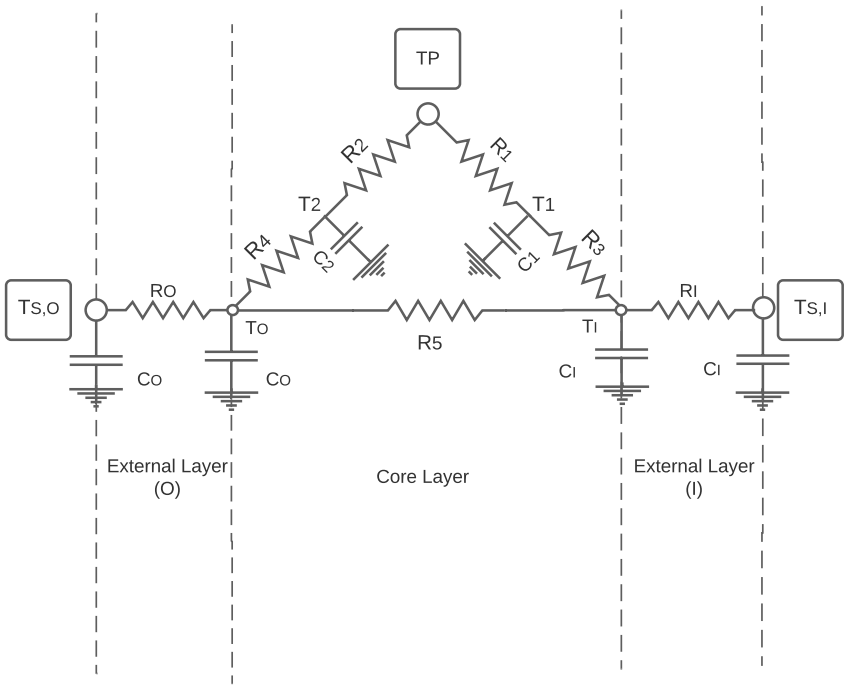

Fig. 3. Delta RC network.

with unknown temperature is written as follows:

$$C_1 \frac{dT_1}{dt} = \frac{T_P - T_1}{R_1} + \frac{T_I - T_1}{R_3}, \tag{9}$$

$$C_2 \frac{dT_2}{dt} = \frac{T_P - T_2}{R_2} + \frac{T_O - T_2}{R_4}, \tag{10}$$

$$C_I \frac{dT_I}{dt} = \frac{T_{S,I} - T_I}{R_I} + \frac{T_O - T_I}{R_5} + \frac{T_1 - T_I}{R_3}, \tag{11}$$

$$C_O \frac{dT_O}{dt} = \frac{T_{S,O} - T_O}{R_O} + \frac{T_I - T_O}{R_5} + \frac{T_2 - T_I}{R_4}. \tag{12}$$

where C [$\mathrm{Jm^{-2}K^{-1}}$] and R [$\mathrm{m^2KW^{-1}}$] are the thermal capacitance and resistance, respectively.

Introducing the temperatures definitions in the frequency domain form (as in Eq. (2)) into Eqs. (9) through (12) and collecting the real and imaginary terms yield the matrix equation (13).

$$\begin{bmatrix}
\frac{1}{R_1}+\frac{1}{R_3} & -C_1\,\omega & 0 & 0 & -\frac{1}{R_3} & 0 & 0 & 0 \\
C_1\,\omega & \frac{1}{R_1}+\frac{1}{R_3} & 0 & 0 & 0 & -\frac{1}{R_3} & 0 & 0 \\
0 & 0 & \frac{1}{R_2}+\frac{1}{R_4} & -C_2\,\omega & 0 & 0 & -\frac{1}{R_4} & 0 \\
0 & 0 & C_2\,\omega & \frac{1}{R_2}+\frac{1}{R_4} & 0 & 0 & 0 & -\frac{1}{R_4} \\
-\frac{1}{R_3} & 0 & 0 & 0 & \frac{1}{R_I}+\frac{1}{R_5}+\frac{1}{R_3} & -C_I\,\omega & -\frac{1}{R_5} & 0 \\
0 & -\frac{1}{R_3} & 0 & 0 & C_I\,\omega & \frac{1}{R_I}+\frac{1}{R_5}+\frac{1}{R_3} & 0 & -\frac{1}{R_5} \\
0 & 0 & -\frac{1}{R_4} & 0 & -\frac{1}{R_5} & 0 & \frac{1}{R_O}+\frac{1}{R_5}+\frac{1}{R_4} & -C_O\,\omega \\
0 & 0 & 0 & -\frac{1}{R_4} & 0 & -\frac{1}{R_5} & C_O\,\omega & \frac{1}{R_O}+\frac{1}{R_5}+\frac{1}{R_4}
\end{bmatrix}
\begin{bmatrix} u_1 \\ v_1 \\ u_2 \\ v_2 \\ u_I \\ v_I \\ u_O \\ v_O \end{bmatrix}
=
\begin{bmatrix} \frac{u_P}{R_1} \\ \frac{v_P}{R_1} \\ \frac{u_P}{R_2} \\ \frac{v_P}{R_2} \\ \frac{u_{S,I}}{R_I} \\ \frac{v_{S,I}}{R_I} \\ \frac{u_{S,O}}{R_O} \\ \frac{v_{S,O}}{R_O} \end{bmatrix} \tag{13}$$

2.3.2. Umbrella RC network model

This novel model configuration in an attempt to combine the performances of the Star and the Delta RC networks. It was observed from the results presented in this article, as will showed later, that the Star model is

able to accurately predict the internal heat fluxes (pipe zone) while the proposed Delta model better predicts the heat fluxes at external surfaces (outside and inside APES surfaces). The proposed Umbrella RC configuration, shown in Fig. 4, is a combined star-triangular model, where the thermal behavior of the core layer is modeled through 8 elements (5 resistances and 3 capacitances). Similarly to the delta configuration, the parameters R_I, R_O, C_I and C_O can be expressed in terms of R_1,...,R_5. The derivation is presented in Appendix B.

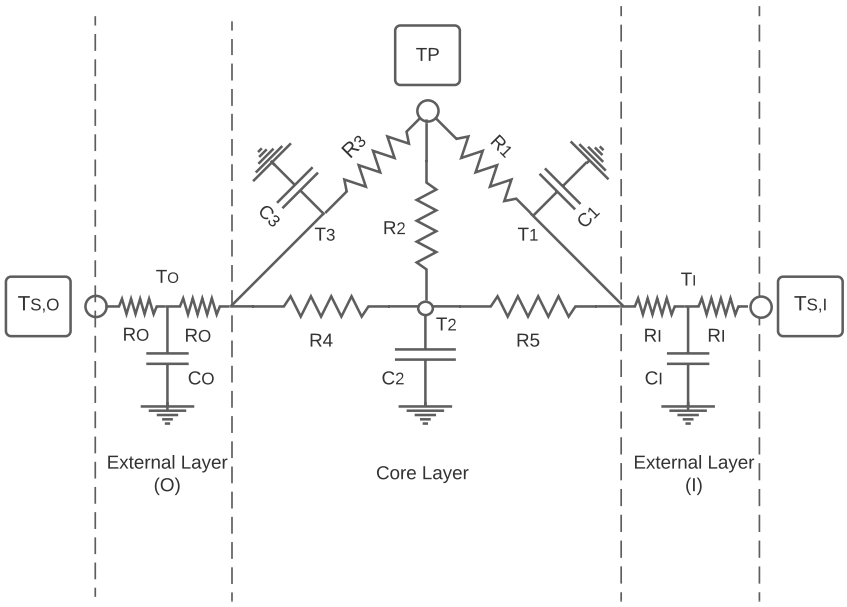

Fig. 4. Umbrella RC network.

The heat balance equations for the Umbrella RC model are given by Eqs. (14) through (18).

$$C_1\frac{dT_1}{dt} = \frac{T_I - T_1}{R_I} + \frac{T_P - T_1}{R_1} + \frac{T_2 - T_1}{R_5}, \tag{14}$$

$$C_2\frac{dT_2}{dt} = \frac{T_1 - T_2}{R_I} + \frac{T_P - T_2}{R_2} + \frac{T_3 - T_2}{R_3}, \tag{15}$$

$$C_3\frac{dT_3}{dt} = \frac{T_O - T_3}{R_O} + \frac{T_P - T_3}{R_3} + \frac{T_2 - T_3}{R_4}, \tag{16}$$

$$C_I\frac{dT_I}{dt} = \frac{T_1 - T_I}{R_I} + \frac{T_2 - T_I}{R_5} + \frac{T_{S,I} - T_I}{R_I}, \tag{17}$$

$$C_O\frac{dT_O}{dt} = \frac{T_3 - T_O}{R_O} + \frac{T_2 - T_O}{R_4} + \frac{T_{S,O} - T_O}{R_O}, \tag{18}$$

Introducing the temperatures definitions in the frequency domain form (as in Eq. (2)) into Eqs. (14) through (18) and collecting the real and imaginary terms yield the following matrix equation:

$$\begin{bmatrix}
\frac{1}{R_I}+\frac{1}{R_1}+\frac{1}{R_5} & -C_1\omega & -\frac{1}{R_5} & 0 & 0 & 0 & 0 & 0 & -\frac{1}{R_I} & 0 \\
C_1\omega & \frac{1}{R_I}+\frac{1}{R_1}+\frac{1}{R_5} & 0 & -\frac{1}{R_5} & 0 & 0 & 0 & 0 & 0 & -\frac{1}{R_I} \\
-\frac{1}{R_5} & 0 & \frac{1}{R_5}+\frac{1}{R_4}+\frac{1}{R_2} & -C_2\omega & -\frac{1}{R_4} & 0 & 0 & 0 & 0 & 0 \\
0 & -\frac{1}{R_5} & C_2\omega & \frac{1}{R_5}+\frac{1}{R_4}+\frac{1}{R_2} & 0 & -\frac{1}{R_4} & 0 & 0 & 0 & 0 \\
0 & 0 & -\frac{1}{R_4} & 0 & \frac{1}{R_O}+\frac{1}{R_4}+\frac{1}{R_3} & -C_3\omega & -\frac{1}{R_O} & 0 & 0 & 0 \\
0 & 0 & 0 & -\frac{1}{R_4} & C_3\omega & \frac{1}{R_O}+\frac{1}{R_4}+\frac{1}{R_3} & 0 & -\frac{1}{R_O} & 0 & 0 \\
0 & 0 & 0 & 0 & -\frac{1}{R_O} & 0 & \frac{2}{R_O} & -C_O\omega & 0 & 0 \\
0 & 0 & 0 & 0 & 0 & -\frac{1}{R_O} & C_O\omega & \frac{2}{R_O} & 0 & 0 \\
-\frac{1}{R_I} & 0 & 0 & 0 & 0 & 0 & 0 & 0 & \frac{2}{R_I} & -C_I\omega \\
0 & -\frac{1}{R_I} & 0 & 0 & 0 & 0 & 0 & 0 & C_I\omega & \frac{2}{R_I}
\end{bmatrix}
\begin{bmatrix} u_1 \\ v_1 \\ u_2 \\ v_2 \\ u_3 \\ v_3 \\ u_O \\ v_O \\ u_I \\ v_I \end{bmatrix}
=
\begin{bmatrix} \frac{u_P}{R_1} \\ \frac{v_P}{R_1} \\ \frac{u_P}{R_2} \\ \frac{v_P}{R_2} \\ \frac{u_P}{R_3} \\ \frac{v_P}{R_3} \\ \frac{u_{S,O}}{R_O} \\ \frac{v_{S,O}}{R_O} \\ \frac{u_{S,I}}{R_I} \\ \frac{v_{S,I}}{R_I} \end{bmatrix} \tag{19}$$

The total number of parameters of the model are eight: R_1 through R_5, C_1, C_2 and C_3. As mentioned before, the parameters R_I, R_O, C_I and C_O of the external layers (2R1C) can be mathematically expressed in terms of R_1 through R_5.

2.4. Calibration of the RC network models through Genetic Algorithm

The calibration of each RC network model can be stated as an optimization problem, which is mathematically equivalent to finding a set of design variables $\mathbf{x} = (x_1, x_2, \ldots, x_n)$ (the set of the resistances (R) and capacitances (C) of each model) that minimize the prediction error (the objective function) of the RC network model regarding the baseline FDFD model,

$$\begin{aligned} &\text{minimize} f(\mathbf{x}) \\ &\text{subjected to :} \\ &x_i^L \leq x_i \leq x_i^U,\ i = 1, \ldots, n; \end{aligned} \tag{20}$$

where x_i^L and x_i^U are the lower and upper bounds for the design variable x_i and f is the objective function defined as follows:

$$f(\mathbf{x}) = \sum_{b=1}^{B} w_b \ \mathrm{nRMSE_b}(\mathbf{x}), \tag{21}$$

where $\mathrm{nRMSE_b}(\cdot, b)$ is the normalized root mean square error of the predicted variable b by the RC network model. The number of variables used in the calibration is $B = 6$, corresponding to the amplitude and phase angle of the heat flux on the outside, pipe, and inside surfaces of the APES system. The weight w_b associated with each of the variables is chosen constant and equal to $1/B$.

The $\mathrm{nRMSE_b}$ values employed in the objective function are calculated according to the following expression

$$\mathrm{nRMSE_b} = \frac{\|\mathrm{b_{FDFD,\omega}} - \mathrm{b_\omega}\|}{\|\mathrm{b_{FDFD,\omega}} - \overline{\mathrm{b_{FDFD,\omega}}}\|}, \tag{22}$$

where $\mathrm{b_{FDFD,\omega}}$ can be the amplitude or phase angle on one of the surface of the APES system (outside, pipe, or inside) for each frequency ω predicted by the baseline FDFD model, and $\mathrm{b_\omega}$ is the corresponding value predicted by the RC network model (5R2C, Star, Delta or Umbrella). The frequency range for the calibration is 10^{-8} to 10^{-3} rad/s with 51 sampled points. This range have demonstrated to be wide enough to cover the dominant frequency components of typical building elements [12, 23].

Computational Implementation. To perform the calibration processes a genetic algorithm (GA) [28] is dynamically coupled with the linear equation system of each RC network in order to solve the problem (20). This choice is based on the fact that GA provides better solutions when functions with multiple local-optima are evaluated; they have low sensitivity to discontinuities in the objective function [29, 30]. Fig. 5 shows a brief description of the parameter calibration process using GA. During each fitness step, the objective $f(\mathbf{x})$ is calculated for each individual $\mathbf{x}$ in the population. That is to say, for each set of RC parameters proposed by the GA, the thermal frequency response of the RC network models is obtained and the objective $f(\mathbf{x})$ is evaluated according to Eq. 21 where the baseline FDFD solution is used. Then, all the set of parameters and their corresponding fitness values are returned to the GA to develop the next generation. This iterative procedure is repeated until one of the stopping criteria is met.

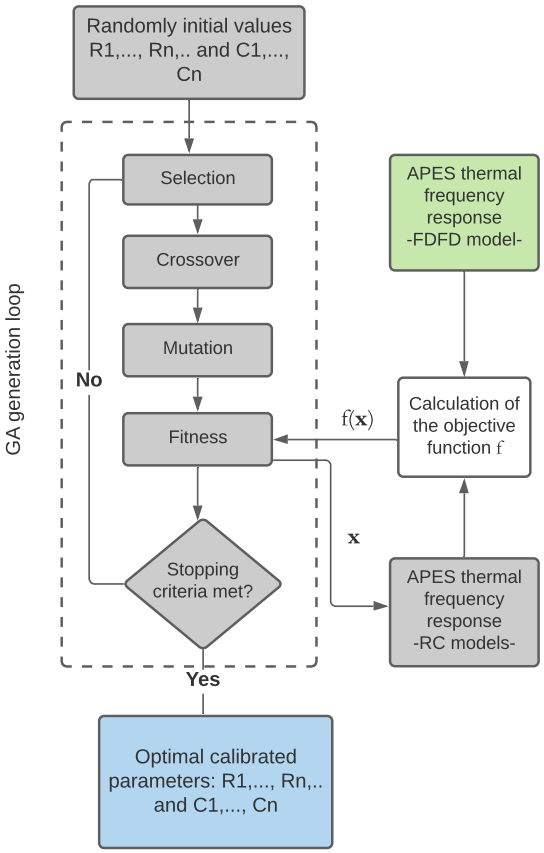

Fig. 5. Flow chart of the calibration process of the RC models through the Genetic Algorithm.

There is not a general rule for choosing the appropriate GA settings: the population size, selection, crossover and mutation methods, probability of mutation and crossover, etc., depending on the characteristics of the optimization problem [29]. However, the probabilities should be kept between the recommended ranges (crossover from 70% to 100% and mutation from 1% to 30%). Therefore, for each model and case study probabilities of 80% and 20% are used for crossover and mutation operation, respectively. On the other hand, since solving the system of linear equations of the RC networks does not demand much computational effort, large populations of 1000 individuals and 100 generations are employed to ensure that the parameters obtained are close to the global optimum and not on the vicinity of local minima.

2.5. Case studies

The methodology described can be replicated for any APES system (with different thermal properties of the concrete layer, different pipe configurations, or for single or multi-layer systems), following the process showed in the Fig. 5. In this effort, to evaluate the performance of the RC network models (the two developed and the two from the current literature) in a wide range of thermal mass applications, three different slab thicknesses are chosen, namely, 40 mm (thin layer), 100 mm (intermediate layer), and 200 mm (thick layer). These single layer systems are made of high density concrete, a typical building construction material [12]. The piping spacing and pipe diameter are 200 mm and 20 mm, respectively. The pipes are placed in the center of the layer. The

thermal conductivity, heat capacity and density of the chosen concrete are 1.731 $Wm^{-1}K^{-1}$, 840 J $kg^{-1}K^{-1}$, 2243 kgm^{-3}, respectively.

3. Results

In this section, the results obtained with the calibrated RC networks for the three case studies are presented and systematically compared against the FDFD results. Then, a detailed comparison between the thermal frequency responses predicted by one the literature models and one of the proposed models is carried out to determine their strengths and weaknesses in reproducing the results of the baseline FDFD model.

3.1. Optimized sets of RC parameters

Table 1 shows the calibrated parameters of all the RC networks and for the three cases studies proposed. Also, the value of the objective function f evaluated at the optimal parameters are included as a general indicator of the agreement between the FDFD baseline model and the different RC network models. So, when smaller is the value of f, better is the accuracy of the RC model regarding the FDFD results. The best model for each case study is underlined.

For the three case studies, the Umbrella RC network outperform the rest of the models. The remaining models show a similar performance for all case studies in term of objective function. For the thin layer (40 mm), the four RC models present good performance after optimization process. For the intermediate layer (100 mm), major differences can be observed in the f values for the different models. In this case, the values of f for the triangular configurations (5R2C and Delta) are lower than the value for the Star RC network, which indicates a better level of agreement with the the baseline results (FDFD). It is worth noting that for the Umbrella model the values of f are at least 40% smaller than for the rest of the models. Regarding the thick layer of 200 mm thickness, the thermal performance of Umbrella RC network is significantly better than the rest of the models in terms of f values. In this case, the values of f for the Star, 5R2C and Delta RC networks are about five times greater than the value for the Umbrella model. In general terms, the 5R2C (literature model) and Umbrella (proposed model) RC networks achieved the best calibration results based on the lower values of f obtained.

3.2. Agreement between the results of the FDFD and the RC networks

The accuracy of the RC network models and their ability replicate the predictions of the FDFD model are judged by analyzing the frequency characteristics of the heat flux through the three key surfaces of the APES system. Due to symmetry, the thermal response of the APES model to the first and second boundary conditions (disturbances) are equivalent. Therefore, only the heat flux frequency response due to boundary conditions (i) and (iii) are analyzed.

In Figs. 6 through 9, predicted-versus-reference scatter plots for the heat flux on the key surfaces of the APES system are presented. In these plots, the predicted and reference heat fluxes due to both boundary conditions across all the frequencies analyzed are included. If the predictions are in full agreement with the reference values, then the points in this plot should lie along the line with slope equal to 1 shown in black. Through these plots, it is, then, possible to evaluate the agreement between the different RC network models and the baseline FDFD model. Te accuracy of the the RC network models is quantitatively evaluated through the normalized

Table 1. R and C parameters and the corresponding $f(\mathbf{x})$ values found after calibration of all RC network models.

Case study	Model	R1	R2	R3	R4	R5	C1	C2	C3	$f(\mathbf{x})$
40 mm	**5R2C**	0.003321	0.018468	0.025242	0.025242	0.003321	37680	37680	-	0.00756
	Star	0.008841	0.000357	4.84E-05	-	-	25741	3957.8	-	0.01122
	Delta	0.023157	0.023157	0.001502	0.001502	0.016478	31962	31962	-	0.00829
	Umbrella	0.067792	0.015624	0.067792	0.006100	0.006100	21541	16145	21541	0.00661
100 mm	**5R2C**	0.011570	0.046773	0.051843	0.051843	0.011570	84271	84271	-	0.02807
	Star	0.000076	0.000480	0.017554	-	-	1008	5738	-	0.03988
	Delta	0.051291	0.051291	0.000822	0.000822	0.046801	51427	51427	-	0.02905
	Umbrella	0.201700	0.024904	0.201700	0.012114	0.012114	16914	44735	16914	0.01668
200 mm	**5R2C**	0.019335	0.156660	0.073144	0.073144	0.019335	174540	174540	-	0.14803
	Star	0.004603	0.019211	1.00E-05	-	-	58642	18615	-	0.14103
	Delta	0.076520	0.076520	0.000010	0.000010	0.152730	1.11E+05	1.11E+05	-	0.15049
	Umbrella	0.286050	0.028525	0.286050	0.034411	0.034411	36726	1.10E+05	36726	0.03366

root mean square error (nRMSE) and the normalized mean bias error (nMBE), which are computed according to the following expressions:

$$\mathrm{nRMSE} = 100\% \, \frac{\|\mathrm{x_{ref,i}} - \mathrm{x_i}\|}{\|\mathrm{x_{ref,i}} - \overline{\mathrm{x_{ref,i}}}\|}, \tag{23}$$

$$\mathrm{nMBE} = 100\% \, \frac{\overline{\mathrm{x_{ref,i}} - \mathrm{x_i}}}{\|\mathrm{x_{ref,i}} - \overline{\mathrm{x_{ref,i}}}\|}, \tag{24}$$

where $\mathrm{x_{ref,i}}$ and $\mathrm{x_i}$ are the baseline model values and the predicted values from the simple RC models, respectively.

In Fig. 6, the agreement between the predictions of the 5R2C network model and the baseline model FDFD is evaluated. Regarding the heat flux amplitude across the key surfaces (Figs. 6a, 6c and 6d), a very good agreement is observed between the 5R2C network model and the FDFD model for the 40 mm thick APES. However, for the thicker APES, the model under predicts the reference values, especially for the thick layer (red triangles). It was observed that the largest deviations between this model and the reference model occur at the high frequencies of the evaluated range. Regarding the heat flux phase angle, some discrepancies between the 5R2C and the FDFD model are observed for all the thickness cases, although these are more pronounced for the thicker APES system. Similarly to the amplitude, the largest deviations of the 5R2C prediction of the phase angle with respect to the reference values occur at high frequencies. The overall values of the nRMSE and the nMBE, obtained by combining all the data for all the boundary conditions evaluated and all the thickness cases are reported in the figures. From those values, it is clear that the 5R2C has the largest errors in the prediction of the amplitude of the heat flux on the outside surface (nRMSE of 7.5%) and the prediction of the the phase angle on the inside surface (nRMSE of 25.2%).

The agreement between the Star RC network model and the baseline model is analyzed in Fig. 7. Judging by the values of nRMSE and nMBE reported in this figure, the accuracy of the amplitude heat flux predictions on outside and inside surfaces is lower than the 5R2C model. As it was the case for the 5R2C network model, the Star model also shows deficiencies in the prediction of the amplitude and especially the phase angle of the heat flux for the thicker APES system and for the high end of the frequencies considered. However, the Star

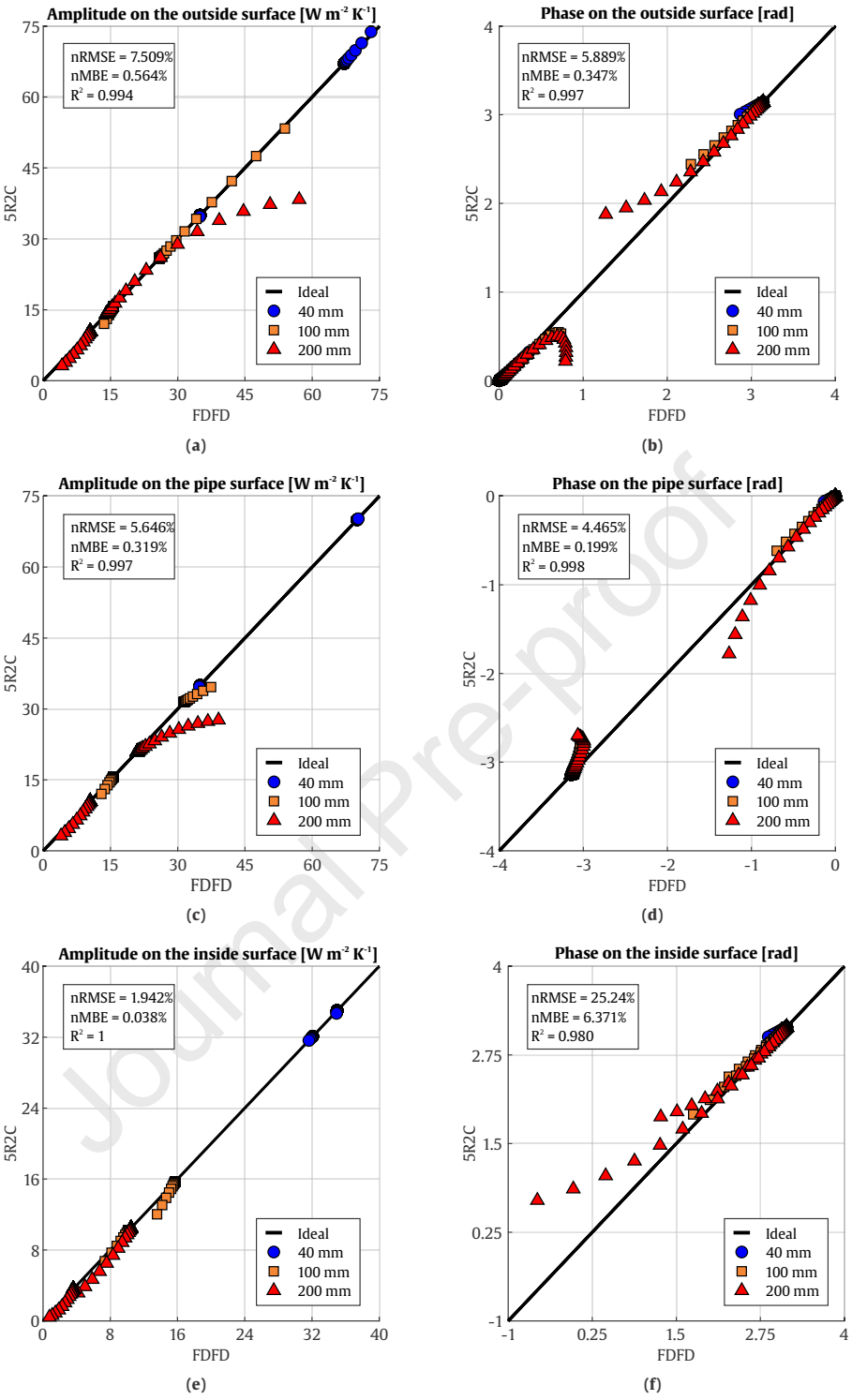

Fig. 6. Predicted-versus-reference plots of the 5R2C network model for the three case studies (thickness) and the two boundary conditions analyzed.

model shows a notable ability to simulate the heat flux amplitude and phase angle on the pipe wall surface for all the cases (nRMSE values of 1.2% and 1.9%, respectively).

For the Delta RC network model, the predicted versus reference scatter plots for the heat flux are presented in Fig. 8. The results for this case are similar to the 5R2C network. A slight improvement in the agreement

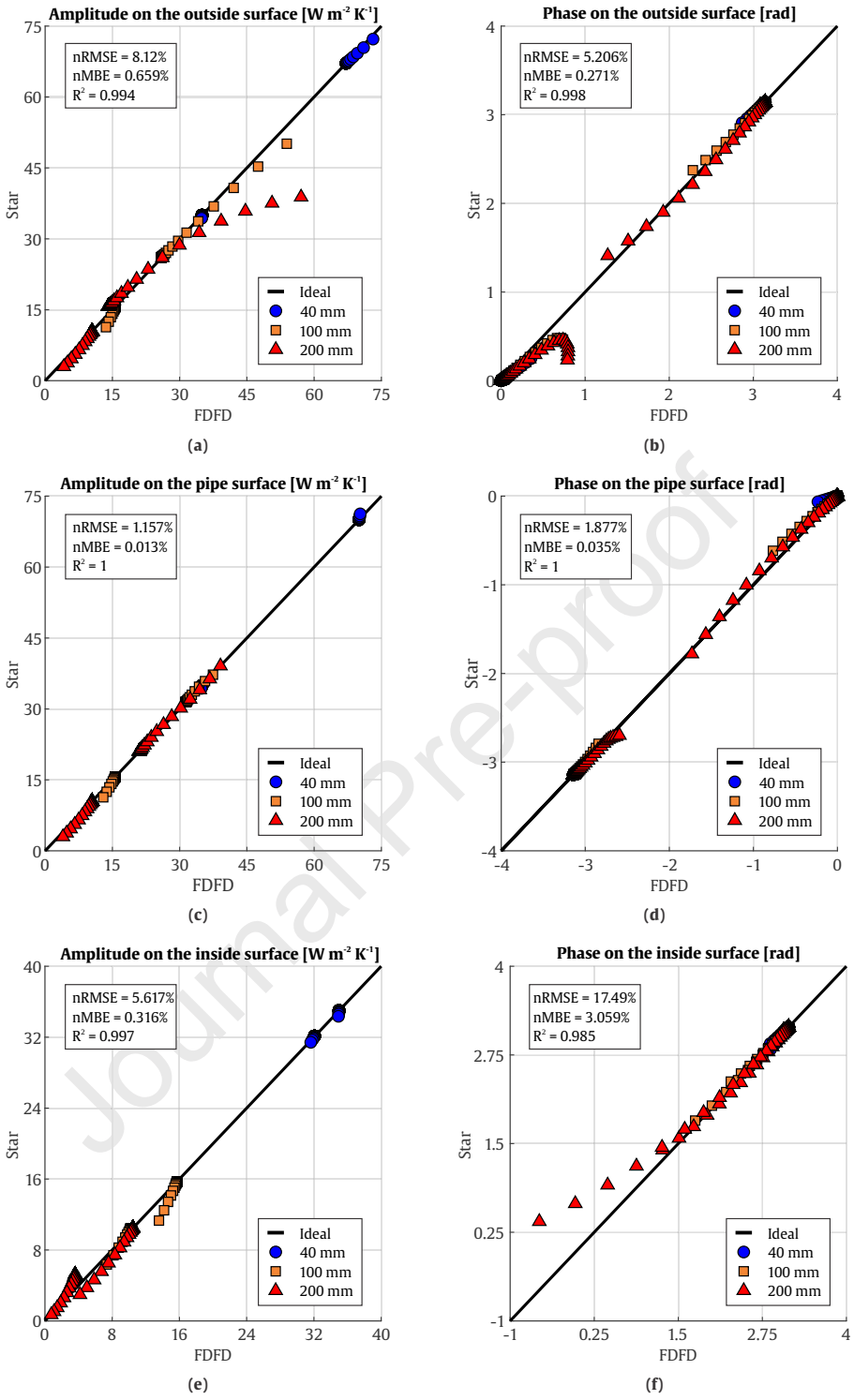

Fig. 7. Predicted-versus-reference plots of the Star RC network model for the three case studies (thickness) and the two boundary conditions analyzed.

for the heat flux amplitudes on the outside and inside surfaces (nRMSE values of 5.2% and 1.4%, respectively) can be observed when compared to the 5R2C predictions. However, a larger dispersion is observed for the heat flux amplitude and phase angle on the pipe wall surface when the thickness of the main layer is 200 mm. It was observed that the largest differences between the model and the reference correspond to the high frequency end

of the analyzed range. Judging the the nRMSE, it is observed that for the inside surface, the predictions of the heat flux phase angle of this model are poorer compared to the previous two models (nRMSE of 34.3%).

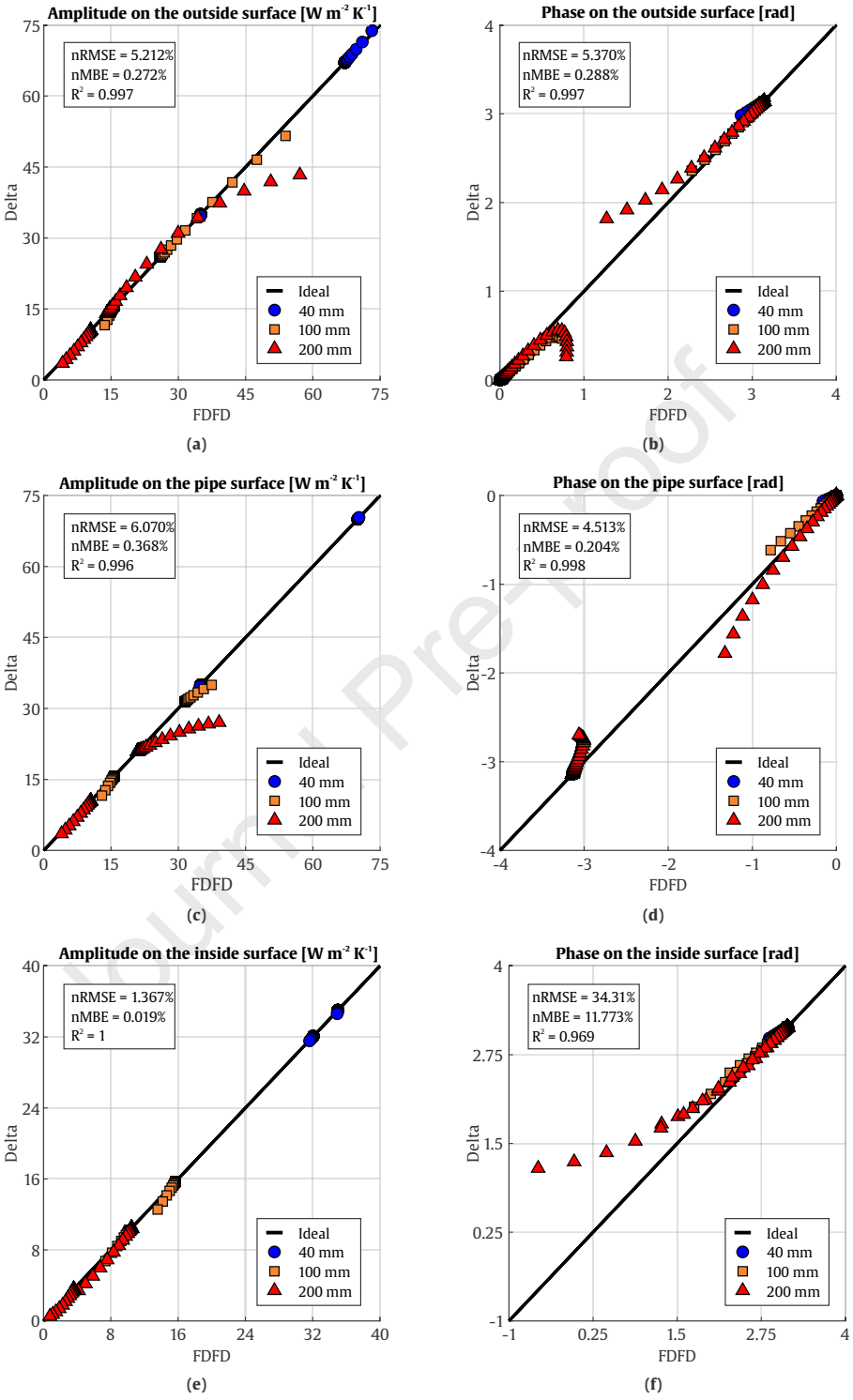

Fig. 8. Predicted-versus-reference plots of the Delta RC network model for the three case studies (thickness) and the two boundary conditions analyzed.

Finally, the Umbrella RC network model is analyzed in Fig. 9. A general improvement with respect to the previous models is observed, which is confirmed by the small values of the nRMSE and the nMBE reported in

the figure. It is noted that, for the heat flux amplitude, the nRMSE values are lower than 1% for all analyzed surfaces. The largest nRMSE and nMBE values correspond to heat flux phase angle predictions on the inside surface, Fig. 9f, but still they are smaller than for the rest of the models. It was determined that this relatively high values are associated to frequencies above 10^{-4} rad/s or periods lower than 17.5 h. For this range, the thermal frequency responses are difficult to accurately capture. As for pipe wall surface, Fig. 9c and 9d, the performance of Umbrella model is as good as the Star model in terms of the nRMSE and nMBE values reported in the figure.

In Table 2 average values of the nRMSE and the nMBE of the predictions of the heat flux amplitudes and phase angles for each model analyzed are reported. These values are obtained by averaging the nRMSE and nMBE reported in Figs. 6 through 9 on the three surfaces of interest for a particular model.

Table 2. Mean values of nRMSE and nMBE for the heat flux amplitude and phase angle averaged over the three surfaces analyzed (outside, inside and pipe wall surfaces).

Model	**Amplitude**		**Phase Angle**	
	nRMSE%	**nMBE%**	**nRMSE%**	**nMBE%**
5R2C	5.0	0.3	11.8	2.3
Star	4.9	0.3	8.2	1.1
Delta	4.2	0.3	14.7	4.1
Umbrella	0.7	0.006	5.3	0.5

3.3. Response in the frequency domain for the thick layer APES

The regression analysis from the previous section highlights the great potential of the Umbrella model for predicting the thermal response of the APES system over a wide range of frequencies and for massive elements (thick layer). The remaining models, 5R2C, Star and Delta RC networks, were observed to have similar performance among them in all of the cases. As mentioned before, the thermal response of the APES system to high frequency fluctuations of the temperature imposed on the key surfaces are not properly captured by the currently available models. This fact is further analyzed in Fig. 10, where the heat flux frequency responses of the thick layer APES system predicted by the 5R2C and Umbrella network models are compared against the FDFD baseline model. In this figure, only the first (i) and third (iii) temperature disturbance boundary conditions, defined in Section 2.1, are considered. In the following description, the heat flux frequency responses are analyzed for each key surface individually.

In general terms, it clear from Fig. 10 that the Umbrella model is able reproduce the amplitude of the heat flux frequency response curves on all the surfaces and for both boundary conditions considered across the entire frequency range analyzed. On the other hand, the 5R2C model fails to reproduce the heat flux amplitude curves for frequencies above 10^{-4} rad/s. Regarding the phase, neither models is able to completely replicate the reference curve for frequencies above 10^{-4} rad/s; however, it is noted that the performance of the Umbrella model in this high frequency range is superior than the performance of the 5R2C model.

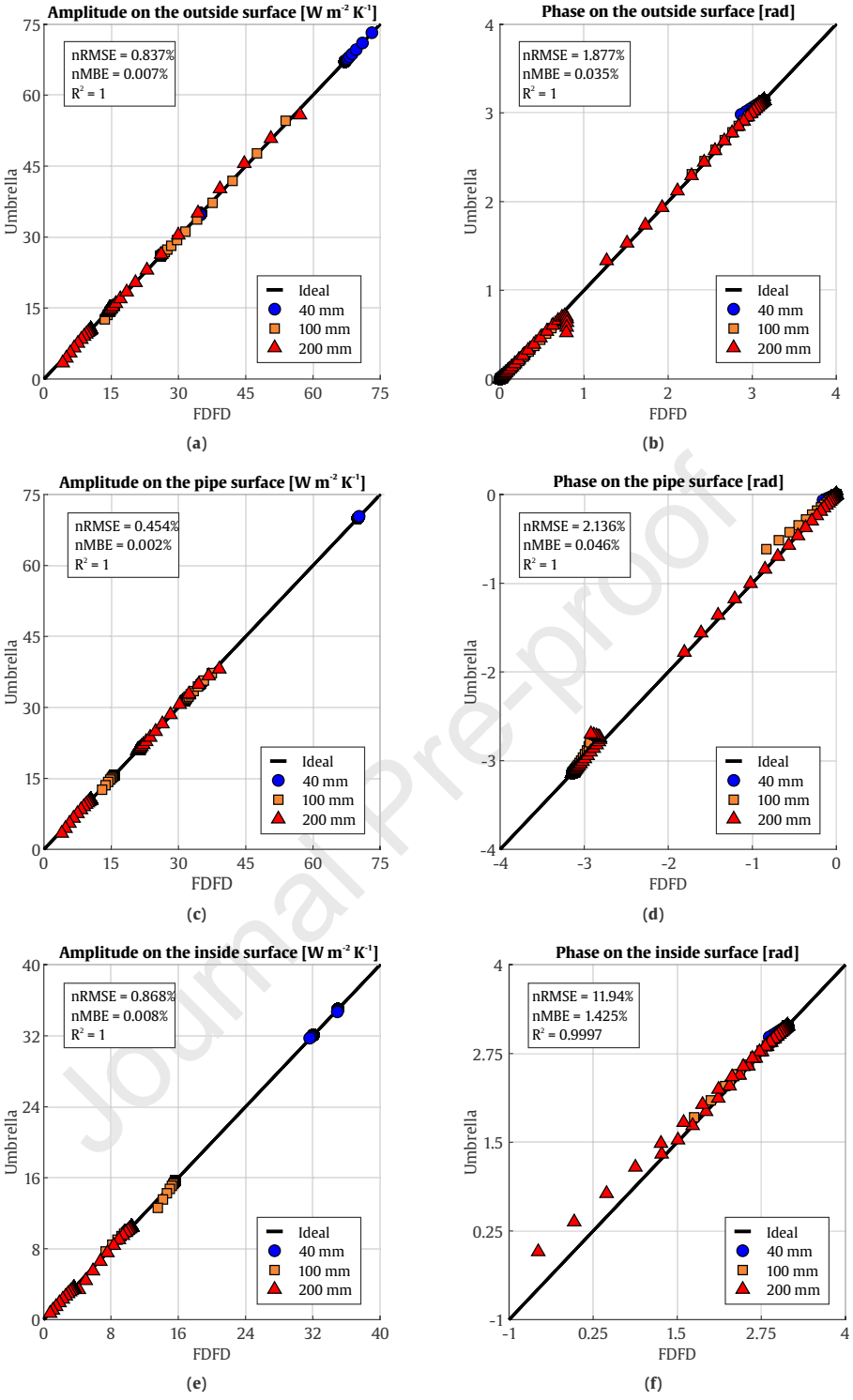

Fig. 9. Predicted-versus-reference plots of the Umbrella RC network model for the three case studies (thickness) and the two boundary conditions analyzed.

Outside Surface. The comparison between the reference and estimated heat flux frequency responses on the outside surface of the APES system is presented in Figs. 10a (amplitude) and 10b (phase lag). In Fig. 10a, it is observed that the Umbrella model (blue circles) is able to reproduce the reference curves throughout the entire frequency range analyzed, for both boundary conditions (i) and (iii). On the other hand, the 5R2C is able

to correctly describe the frequency response of the system due to both temperature disturbances throughout most of the frequency range analyzed except at frequencies $\omega > 10^{-4}$ rad/s where some discrepancies between this model and the reference curve are noted when the input temperature disturbance is applied on the outside surface. The mean relative errors between the predicted and baseline heat flux amplitudes, combining both input conditions are 3.2% for the 5R2C model and 0.8% for the Umbrella model. Regarding the phase lag, Fig. 10b, it is observed that both models replicate correctly the reference curve for frequencies below 10^{-4} rad/s. The Umbrella RC model is able to reproduce the phase angle frequency signature due one of the boundary conditions (condition (iii)) across all the frequency range analyzed; however, it shows some deficiencies for the remaining boundary condition (condition (i)) at frequencies above 10^{-4} rad/s. On the other hand, the 5R2C model fails to replicate the phase curve for both boundary conditions at frequencies higher above 10^{-4} rad/s. This observations are confirmed by the values of the mean relative errors, 16.2% and 4.5% for the 5R2C and Umbrella RC network models, respectively.

Pipe Surface. In terms of the amplitude of the heat flux predictions (Fig. 10c), the same observations as for the outside surface apply regarding the Umbrella RC model. That is to say, this model is able to reproduce the baseline curves across all the frequency range analyzed. The 5R2C model, as in the previous case, also shows noticeable deficiencies for frequencies above 10^{-4} rad/s, but in this case, when the input temperature disturbance is applied on the pipe wall surface itself. Also, a slight offset is observed on the low frequency range below 10^{-4} rad/s for this particular disturbance case. The mean relative errors corresponding to the predictions of the heat flux amplitude on this surface are 4.4% and 0.5%, for the 5R2C and Umbrella RC network models, respectively. Regarding the phase lag, Fig. 10d, the same observations as before for frequencies below 10^{-4} rad/s apply for both models. In this case, the mean relative errors are 41.0% and 6.4% for the the 5R2C and Umbrella RC network models, respectively.

Inside Surface. From Fig. 10e it is observed that both models correctly capture the baseline amplitude frequency curves. However, as it was pointed out for the pipe wall surface, the 5R2C network model shows a slight constant offset mostly on the low frequency range. Regarding the heat flux phase lag across this surface, the same observations as in the previous cases are made on Fig. 10f. For this surface, the values of the mean relative errors of the 5R2C and Umbrella RC network models are: 6.8% and 1.1% for the heat flux amplitude, and 12.4% and 5.2% for the heat flux phase lag, respectively.

4. Discussion

From the results analyzed in the previous sections, it can be observed that the layer massiveness, which is associated with the layer thickness, considerably affects the accuracy of the RC models. For the thin layer (40 mm), the performance of the all models is reliable for all disturbances conditions. This observation is also confirmed by the small final values (around around 0.01) that the objective function takes for all the models. However, it was observed that, in general, the ability of the models to reproduce the baseline system worsens for the intermediate and thick layers (100 mm and 200 mm). The results show that the Star RC model can accurately predict the amplitude and phase angle of the heat flux on the pipe surface for all the cases analyzed,

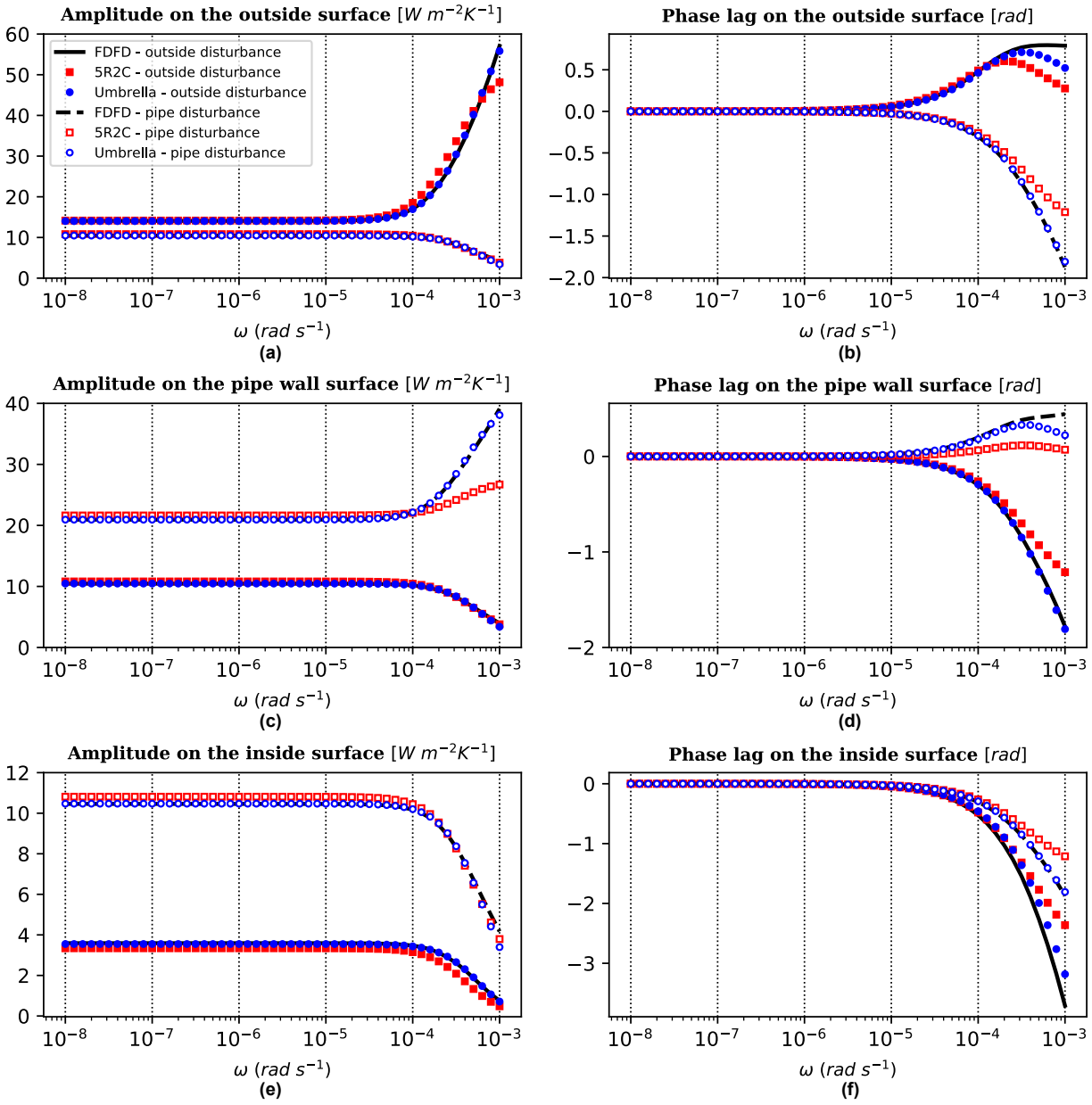

Fig. 10. Comparison in the frequency domain between the predictions of the 5R2C and Umbrella RC network models and the FDFD baseline model considering the first (i) and third (iii) temperature disturbance conditions, i.e. thermal periodic excitation on the outside and pipe wall surfaces, respectively.

with a mean nRMSE value of 1.5% while the mean nRMSE value was around 5% for the triangular models). On the other hand, the 5R2C and Delta networks yield more accurate values of the heat flux amplitude across the APES faces (outside and inside surfaces) with mean nRMSE values of 4.7% and 3.3% respectively, against 6.9% for the Star model. However, for the heat flux phase angle predictions, the performance of these triangular RC networks is worse than the Star network (nRMSE values of 15.5% and 18.8% for the 5R2C and Delta models respectively, against 11.3% for the Star model).

According to the data shown in Table 2, the Delta RC-network yields smaller values of overall nRMSE for the heat flux amplitude prediction compared to the 5R2C and Star networks. Nevertheless, for the heat flux phase

angle predictions, the performance of the Delta model is slightly worse than the rest. The proposed combined model, the Umbrella RC network, was shown to give better estimations of the APES thermal behavior than the rest of the models analyzed in this article. For all the cases, the values of the nRMSE corresponding to the prediction of the heat flux amplitude are less than 1%. For the heat flux phase angle, the nRMSE values are close to 2% for the outside and pipe surfaces, and 12% on the inside surface. These values indicate that dynamic thermal behavior is accurately predicted by the Umbrella network for thin, intermediate and thick layers. From the frequency responses of the APES systems, it is observed that the critical range of frequencies are between 10^{-4} and 10^{-3} rad/s. In this range, the frequency response curves of the APES systems depict a larger variation with the frequency, which cannot be correctly captured by the previous models in the literature. The proposed Umbrella network model; however, was able to reproduce very closely this behavior, thus outperforming the rest of models in this critical frequency range.

5. Conclusions

In this work, two novel thermal models, referred to as Delta and Umbrella RC-networks, are presented to evaluate the thermal behavior of the main layer of active pipe-embedded structures (APES). In order to assess the quality of the proposed models and other models available in the literature, a high-fidelity two-dimensional Frequency-Domain finite-difference model (FDFD) was employed to generate reliable estimations of the frequency characteristics of the APES system analyzed. The parameters of the RC network models, i.e. thermal resistances and capacitances, were determined through an optimization method based on a genetic algorithm. This parameter identification process was dynamically coupled with the simplified models to find the RC parameters that allow to best reproduce the frequency response characteristics of the baseline FDFD model. The thermal behavior of three concrete layers with different thicknesses, 40 mm, 100 mm, and 200 mm, representative of a thin, intermediate and thick layer, respectively, were studied to evaluate the performance of the simplified models.

As general conclusion, it was observed that the performance of all the RC models decreased with the layer thickness or massiveness. For the thinner layer (40 mm) all the models accurately represented the dynamic thermal behavior of the system. On the other hand, for the intermediate and thick layers, the accuracy of the models declined in the critical frequency range above 10^{-4} rad/s.

It was found that proposed Delta RC network model has similar performance to the Star and 5R2C models, with overall nRMSE values between 6% and 10%. The Delta model yielded a slight improvement in the prediction of the amplitude of the heat flux across most of the key surfaces of the APES system compared to the literature models.

The Umbrella RC network model, on the other hand, showed a remarkable prediction performance for all the thermal fluctuations inputs considered and across all analyzed key surfaces with an overall nRMSE value of 3%. In comparison with the rest of the models, it was able to better predict the frequency response of the intermediate and, especially the thick layer system within the critical frequency range. In fact, for the 200 mm-thickness layer, the mean nRMSE values for the 5R2C, Star and Delta models are higher than 12%, whereas it is roughly 3% for the Umbrella model. Based on these observations, the Umbrella model is proposed as an

improved model for simulating the thermal behavior of concrete layers with medium to large thickness, which are commonly used in slabs and floors with APES radiant systems.

It is noted that the conclusions of this work apply only to slab thickness ranging from 40 to 200 mm and for thermal perturbations within a frequency range between 10^{-8} to 10^{-3} rad/s. Due to the nature of the frequency domain analysis, transient conditions due to sudden changes in water temperature and heat gains, for instance, whose analysis must be carried out in the time domain, were not considered in the present effort but will constitute future studies. Also, future efforts will explore different APES configurations in order to obtain correlations of the RC-network parameters as function of the inputs parameters (thermal diffusivity of the concrete layer, piping characteristics within the main layer, and so on). This correlations will relieve the end user of the models from the need of the Genetic Algorithm.

The proposed models may be incorporated into available building simulation software to assess the energy performance of buildings with integrated APES systems. This coupling process will be addressed as part of future research.

Acknowledgments

For funding this work, we would like to the National Agency for Scientific and Technological Promotion (ANPCyT), Argentina, via the projects PICT-2018 N°04124 and PICT-2018 N°03252, and also to the National University of Salta via project CIUNSa N°2575.

Appendix A. Finite Difference scheme for spatial discretization

A semi-discrete (method of lines) approach is employed to approximate the governing two-dimensional heat equation by a set of ordinary differential equations (ODEs). To this end, only the spatial derivatives of the heat fluxes q''_x and q''_y in Eq. 1 are discretized by means of the three-point central difference operator for the first order derivative. The spatial derivatives of the heat fluxes at a central cell node i,j is approximated as follows:

$$\frac{\partial q''_{x_{i,j}}}{\partial x} \approx \frac{1}{dx_{i,j}} \left(q''_{x_{i,j+\frac{1}{2}}} - q''_{xi,j-\frac{1}{2}} \right) + \mathcal{O}(dx^2) \tag{A.1}$$

$$\frac{\partial q''_{y_{i,j}}}{\partial y} \approx \frac{1}{dy_{i,j}} \left(q''_{y_{i+\frac{1}{2},j}} - q''_{yi-\frac{1}{2},j} \right) + \mathcal{O}(dy^2) \tag{A.2}$$

where $q''_{i,j\pm\frac{1}{2}}$ and $q''_{i\pm\frac{1}{2},j}$ are the heat fluxes across the faces of the cell i, j. These fluxes are computed by considering two thermal resistances in series connecting the adjacent cell centers and subjected to the temperature differences between those nodes, as shown in Fig. A.11. Therefore,

$$q''_{x_{i,j+\frac{1}{2}}} \approx -\frac{T_{i,j+1} - T_{i,j}}{\frac{dx_{i,j}}{2k_{i,j}} + \frac{dx_{i,j+1}}{2k_{i,j+1}}} \qquad q''_{x_{i,j-\frac{1}{2}}} \approx -\frac{T_{i,j} - T_{i,j-1}}{\frac{dx_{i,j}}{2k_{i,j}} + \frac{dx_{i,j-1}}{2k_{i,j-1}}} \tag{A.3}$$

$$q''_{y_{i+\frac{1}{2},j}} \approx -\frac{T_{i+1,j} - T_{i,j}}{\frac{dy_{i,j}}{2k_{i,j}} + \frac{dy_{i+1,j}}{2k_{i+1,j}}} \qquad q''_{y_{i-\frac{1}{2},j}} \approx -\frac{T_{i,j} - T_{i-1,j}}{\frac{dy_{i,j}}{2k_{i,j}} + \frac{dy_{i-1,j}}{2k_{i-1,j}}} \tag{A.4}$$

where $dx_{i,j}$ and $dy_{i,j}$ are the dimensions of cell i,j (Fig. A.11) and $k_{i,j}$ is the thermal conductivity of cell i,j. The terms in the denominator are the equivalent thermal resistances between nodes i, j and $i, j \pm 1$ and between nodes i, j and $i \pm 1, j$. Combining Eqs. (A.1) through (A.4), the resulting ODE for node i, j is given by:

$$dx_{i,j}dy_{i,j}\rho c_p\frac{\partial T_{i,j}}{\partial t} = dy_{i,j}\frac{T_{i,j+1}-T_{i,j}}{\frac{dx_{i,j}}{2k_{i,j}}+\frac{dx_{i,j+1}}{2k_{i,j+1}}} - dy_{i,j}\frac{T_{i,j}-T_{i,j-1}}{\frac{dx_{i,j}}{2k_{i,j}}+\frac{dx_{i,j-1}}{2k_{i,j-1}}} + dx_{i,j}\frac{T_{i,j+1}-T_{i,j}}{\frac{dy_{i,j}}{2k_{i,j}}+\frac{dy_{i+1,j}}{2k_{i+1,j}}} - dx_{i,j}\frac{T_{i,j}-T_{i-1,j}}{\frac{dy_{i,j}}{2k_{i,j}}+\frac{dy_{i-1,j}}{2k_{i-1,j}}} \quad \text{(A.5)}$$

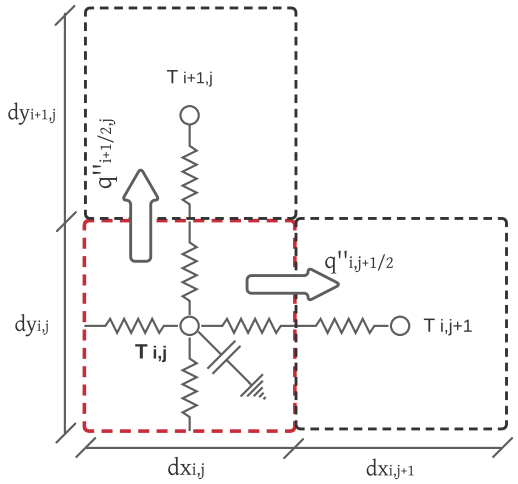

Fig. A.11. Details of the finite difference scheme

Appendix B. Determination of equivalent networks by a steady-state analysis

The thermal parameters to represent the external layers in Delta and Umbrella models can be expressed as functions of the main RC parameters. Following the approach proposed by [23] for a Star RC network, the following mathematical formulation is developed for the Umbrella RC. This approach may be analogously applied to Delta RC configuration.

Analyzing the thermal behavior of the Umbrella RC network when the frequencies are close to 0 rad/s, the thermal RC network shown in Fig. 4 can be transformed into a purely resistive circuit composed of two symmetrical triangular networks, as shown in Fig. B.12a. The well know *delta-star conversion* can be applied to this configuration for simplifying the original complex network. The resistance parameters of the equivalent resistive network shown in Fig. B.12b can be obtained as follows

$$\mathrm{R_{a1}} = \frac{\mathrm{R_1}\,2\mathrm{R_2}}{2\mathrm{R_2}+\mathrm{R_1}+\mathrm{R_5}} \quad \text{(B.1)}$$

$$\mathrm{R_{a2}} = \frac{\mathrm{R_3}\,2\mathrm{R_2}}{2\mathrm{R_2}+\mathrm{R_3}+\mathrm{R_4}} \quad \text{(B.2)}$$

$$\mathrm{R_b} = \frac{\mathrm{R_5}\,2\mathrm{R_2}}{2\mathrm{R_2}+\mathrm{R_1}+\mathrm{R_5}} + \frac{\mathrm{R_4}\,2\mathrm{R_2}}{2\mathrm{R_2}+\mathrm{R_3}+\mathrm{R_4}} \quad \text{(B.3)}$$

$$\mathrm{R_{c1}} = \frac{\mathrm{R_1}\,\mathrm{R_5}}{2\mathrm{R_2}+\mathrm{R_1}+\mathrm{R_5}} \quad \text{(B.4)}$$

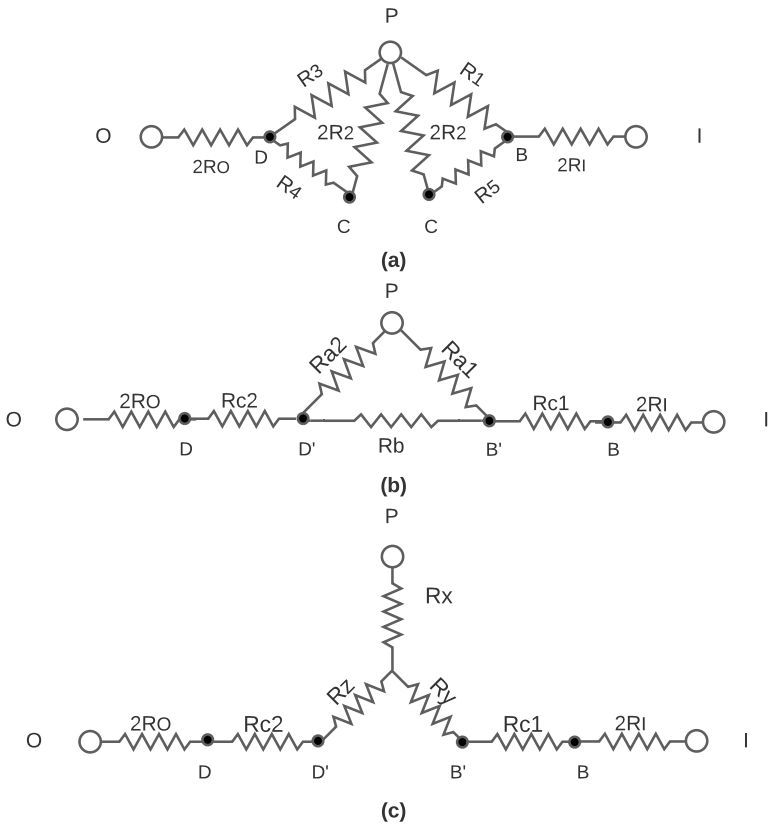

Fig. B.12. Thermal resistive network for Umbrella RC configuration for steady-state analysis

$$R_{c2} = \frac{R_3\, R_5}{2R_2 + R_3 + R_4} \tag{B.5}$$

To further reduce the resultant network to the configuration observed in Fig. B.12c, the equivalent resistances R_x, R_y and R_z are defined as follows:

$$R_x = \frac{R_{a1}\, R_{a2}}{R_{a1} + R_{a2} + R_b} \tag{B.6}$$

$$R_y = \frac{R_{a1}\, R_b}{R_{a1} + R_{a2} + R_b} \tag{B.7}$$

$$R_z = \frac{R_{a2}\, R_b}{R_{a1} + R_{a2} + R_b} \tag{B.8}$$

A general equivalent resistance R_{EQ} can be defined as Eq. (B.9), where R'_y is the equivalent in series of R_y, R_{c1} and $2R_I$ while the equivalent in series of R_z, R_{c2} and $2R_O$ corresponds to R'_z. The ratio between the heat flux q_O^P and q_I^P along the branches P-O and P-I, respectively, is denoted β and given in Eq. (B.10).

$$R_{EQ} = R_x + \frac{R'_y\, R'_z}{R'_y + R'_z} \tag{B.9}$$

$$\beta = \frac{q_O^P}{q_I^P}\Big|_{\omega \to 0} = \frac{R'_y}{R'_z} \tag{B.10}$$

Considering the third disturbance condition (temperature fluctuation imposed on the pipe wall surface), the nodes O and I in Fig. B.12a are at 0 potential. So, the equivalent resistance R_{EQ} could also be determined as the temperature difference ΔT between the nodes T_P and T_O or T_I (1 K) divided by the heat flux from node T_P to the nodes at 0 potential, as indicates Eq. (B.11). The heat fluxes q_P^P, q_O^P and q_I^P are obtained from the FDFD model, for frequencies close to 0 rad/s. Then, the Eqs. (B.12)-(B.13) are obtained to express R_I and R_O, respectively.

$$R_{EQ} = \frac{\Delta T}{q_P^P}\Big|_{\omega \to 0} \tag{B.11}$$

$$R_I = 0.5\left[\left(\frac{\Delta T}{q_P^P}\Big|_{\omega \to 0} - R_x\right)(1+\beta) - R_y - R_{c1}\right] \tag{B.12}$$

$$R_O = 0.5\left[\left(\frac{\Delta T}{q_P^P}\Big|_{\omega \to 0} - R_x\right)(1+1/\beta) - R_z - R_{c2}\right] \tag{B.13}$$

The heat capacities for the external layers C_I and C_O are easily calculated as:

$$C_I = R_I\, k_c\, \rho_c\, c_{p,c}\ ,\ C_O = R_O\, k_c\, \rho_c\, c_{p,c} \tag{B.14}$$

[1] International Energy Agency. World energy balances 2020, 2020.

[2] United Nations Environment Programme. 2020 global status report for buildings and construction: Towards a zero-emission, efficient and resilient buildings and construction sector, 2020.

[3] G.A. Florides, S.A. Tassou, S.A. Kalogirou, and L.C. Wrobel. Review of solar and low energy cooling technologies for buildings. *Renewable and Sustainable Energy Reviews*, 6(6): 557–572, 2002. ISSN 1364-0321. doi: https://doi.org/10.1016/S1364-0321(02)00016-3. URL https://www.sciencedirect.com/science/article/pii/S1364032102000163.

[4] A. Ucar and M. Inalli. A finite element model of solar heating system with underground storage. *International Journal of Thermal Sciences*, 47(12):1639–1646, 2008. ISSN 1290-0729. doi: https://doi.org/10.1016/j.ijthermalsci.2007.12.002. URL https://www.sciencedirect.com/science/article/pii/S1290072907002578.

[5] L. Zhou and C. Li. Study on thermal and energy-saving performances of pipe-embedded wall utilizing low-grade energy. *Applied Thermal Engineering*, 176:115477, 2020. ISSN 1359-4311. doi: https://doi.org/10.1016/j.applthermaleng.2020.115477. URL https://www.sciencedirect.com/science/article/pii/S1359431120329598.

[6] D.G. Leo Samuel, S.M. Shiva Nagendra, and M. Prakash Maiya. Parametric analysis on the thermal comfort of a cooling tower based thermally activated building system in tropical climate – an experimental study. *Applied Thermal Engineering*, 138:325–335,

2018. ISSN 1359-4311. doi: https://doi.org/10.1016/j.applthermaleng.2018.04.077. URL https://www.sciencedirect.com/science/article/pii/S1359431117359343.

[7] M.C. Guerrero Delgado, J. Sánchez Ramos, S. Álvarez Domínguez, J.A. Tenorio Ríos, and L.F. Cabeza. Building thermal storage technology: Compensating renewable energy fluctuations. *Journal of Energy Storage*, 27:101147, 2020. ISSN 2352-152X. doi: https://doi.org/10.1016/j.est.2019.101147. URL https://www.sciencedirect.com/science/article/pii/S2352152X19305468.

[8] J. Oravec, O. Šikula, M. Krajčík, M. Arıcı, and M. Mohapl. A comparative study on the applicability of six radiant floor, wall, and ceiling heating systems based on thermal performance analysis. *Journal of Building Engineering*, 36:102133, 2021. ISSN 2352-7102. doi: https://doi.org/10.1016/j.jobe.2020.102133. URL https://www.sciencedirect.com/science/article/pii/S2352710220337657.

[9] J. Romaní, A. de Gracia, and L.F. Cabeza. Simulation and control of thermally activated building systems (tabs). *Energy and Buildings*, 127:22–42, 2016. ISSN 0378-7788. doi: https://doi.org/10.1016/j.enbuild.2016.05.057. URL https://www.sciencedirect.com/science/article/pii/S0378778816304261.

[10] C. Shen and X. Li. Energy saving potential of pipe-embedded building envelope utilizing low-temperature hot water in the heating season. *Energy and Buildings*, 138:318–331, 2017. ISSN 0378-7788. doi: https://doi.org/10.1016/j.enbuild.2016.12.064. URL https://www.sciencedirect.com/science/article/pii/S0378778816319685.

[11] M. Krajčík, M. Arıcı, O. Šikula, and M. Šimko. Review of water-based wall systems: Heating, cooling, and thermal barriers. *Energy and Buildings*, 253:111476, 2021. ISSN 0378-7788. doi: https://doi.org/10.1016/j.enbuild.2021.111476. URL https://www.sciencedirect.com/science/article/pii/S037877882100760X.

[12] Q. Zhu, X. Xu, J. Wang, and F. Xiao. Development of dynamic simplified thermal models of active pipe-embedded building envelopes using genetic algorithm. *International Journal of Thermal Sciences*, 76:258–272, 2014. ISSN 1290-0729. doi: https://doi.org/10.1016/j.ijthermalsci.2013.09.008. URL https://www.sciencedirect.com/science/article/pii/S1290072913002354.

[13] K.A. Antonopoulos, M. Vrachopoulos, and C. Tzivanidis. Experimental and theoretical studies of space cooling using ceiling-embedded piping. *Applied Thermal Engineering*, 17(4):351–367, 1997. ISSN 1359-4311. doi: https://doi.org/10.1016/S1359-4311(96)00040-3. URL https://www.sciencedirect.com/science/article/pii/S1359431196000403.

[14] R. Holopainen, P. Tuomaala, and J. Piippo. Uneven gridding of thermal nodal networks in floor heating simulations. *Energy and Buildings*, 39(10):1107–1114, 2007. ISSN 0378-7788. doi: https://doi.org/10.1016/j.enbuild.2006.12.006. URL https://www.sciencedirect.com/science/article/pii/S0378778806002994.

[15] M. Krzaczek and Z. Kowalczuk. Thermal barrier as a technique of indirect heating and cooling for residential buildings. *Energy and Buildings*, 43(4):823–837, 2011. ISSN 0378-7788. doi: https://doi.org/10.1016/j.enbuild.2010.12.002. URL https://www.sciencedirect.com/science/article/pii/S0378778810004226.

[16] Z. Tian, B. Duan, X. Niu, Q. Hu, and J. Niu. Establishment and experimental validation of a dynamic heat transfer model for concrete radiant cooling slab based on reaction coefficient method. *Energy and Buildings*, 82:330–340, 2014. ISSN 0378-7788. doi: https://doi.org/10.1016/j.enbuild.2014.07.031. URL https://www.sciencedirect.com/science/article/pii/S0378778814005696.

[17] W. Wu, W. Zhang, J. Benner, and A. Malkawi. Critical evaluation of analytical methods for thermally activated building systems. *Renewable and Sustainable Energy Reviews*, 117:109516, 2020. ISSN 1364-0321. doi: https://doi.org/10.1016/j.rser.2019.109516. URL https://www.sciencedirect.com/science/article/pii/S1364032119307245.

[18] M. Koschenz and V. Dorer. Interaction of an air system with concrete core conditioning. *Energy and Buildings*, 30(2):139–145, 1999. ISSN 0378-7788. doi: https://doi.org/10.1016/S0378-7788(98)00081-4. URL https://www.sciencedirect.com/science/article/pii/S0378778898000814.

[19] K. Liu, Z. Tian, C. Zhang, Y. Ding, and W. Wang. Establishment and validation of modified star-type rc-network model for concrete core cooling slab. *Energy and Buildings*, 43(9): 2378–2384, 2011. ISSN 0378-7788. doi: https://doi.org/10.1016/j.enbuild.2011.05.029. URL https://www.sciencedirect.com/science/article/pii/S037877881100243X.

[20] T. Yu, P. Heiselberg, B. Lei, and M. Pomianowski. Validation and modification of modeling thermally activated building systems (tabs) using energyplus. *Building Simulation*, 7:615–627, 2014. doi: 10.1007/s12273-014-0183-6.

[21] Q. Zhu, X. Xu, and J. Yu. Study of dynamic thermal performance of active pipe-embedded building envelopes based on frequency-domain finite-difference method. *ASim 2012 IBPSA Asia Conference, Shanghai*, 2012. URL http://www.ibpsa.org/proceedings/asim2012/0127.pdf.

[22] Q. Zhu, X. Xu, J. Gao, and F. Xiao. A semi-dynamic model of active pipe-embedded building envelope for thermal performance evaluation. *International Journal of Thermal Sciences*, 88: 170–179, 2015. ISSN 1290-0729. doi: https://doi.org/10.1016/j.ijthermalsci.2014.09.014. URL https://www.sciencedirect.com/science/article/pii/S1290072914002725.

[23] A. Li, Y. Sun, and X. Xu. Development of a simplified resistance and capacitance (rc)-network model for pipe-embedded concrete radiant floors. *Energy and Buildings*, 150: 353–375, 2017. ISSN 0378-7788. doi: https://doi.org/10.1016/j.enbuild.2017.06.011. URL https://www.sciencedirect.com/science/article/pii/S0378778816312749.

[24] T. Weber and G. Jóhannesson. An optimized rc-network for thermally activated building components. *Building and Environment*, 40(1):1–14, 2005.

ISSN 0360-1323. doi: https://doi.org/10.1016/j.buildenv.2004.04.012. URL https://www.sciencedirect.com/science/article/pii/S0360132304001544.

[25] T. Yan, X. Xu, J. Gao, Y.g Luo, and J. Yu. Performance evaluation of a pcm-embedded wall integrated with a nocturnal sky radiator. *Energy*, 210:118412, 2020. ISSN 0360-5442. doi: https://doi.org/10.1016/j.energy.2020.118412. URL https://www.sciencedirect.com/science/article/pii/S036054422031519X.

[26] T. Yan, J. Gao, X. Xu, T. Xu, Z. Ling, and J. Yu. Dynamic simplified pcm models for the pipe-encapsulated pcm wall system for self-activated heat removal. *International Journal of Thermal Sciences*, 144:27–41, 2019. ISSN 1290-0729. doi: https://doi.org/10.1016/j.ijthermalsci.2019.05.015. URL https://www.sciencedirect.com/science/article/pii/S1290072918315370.

[27] F. P. Incropera and D. P. DeWitt. Two-Dimensional, Steady-State Conduction. In *Fundamentals of Heat and Mass Transfer*, chapter 4. John Wiley & Sons, Inc., New York City, New York, 4th edition edition, 1996.

[28] D. E. Goldberg. *Genetic Algorithms in Search, Optimization and Machine Learning*. Addison-Wesley Longman Publishing Co., Inc., 1st. edition, 1989. ISBN 0201157675.

[29] F. Bre, A. S. Silva, E. Ghisi, and V. D. Fachinotti. Residential building design optimisation using sensitivity analysis and genetic algorithm. *Energy and Buildings*, 133:853 – 866, 2016. ISSN 0378-7788. doi: https://doi.org/10.1016/j.enbuild.2016.10.025.

[30] J. M. Gimenez and F. Bre. Optimization of rans turbulence models using genetic algorithms to improve the prediction of wind pressure coefficients on low-rise buildings. *Journal of Wind Engineering and Industrial Aerodynamics*, 193:103978, 2019. ISSN 0167-6105. doi: https://doi.org/10.1016/j.jweia.2019.103978.

Author Contributions

Marcos Hongn: Conceptualization, Methodology, Software, Validation, Formal analysis, Investigation, Writing – original draft preparation, Funding acquisition. **Facundo Bre**: Conceptualization, Methodology, Software, Validation, Formal analysis, Visualization, Writing – reviewing and editing. **Marcelo Valdez:** Conceptualization, Methodology, Writing – reviewing and editing. **Silvana Flores-Larsen:** Conceptualization, Supervision, Writing – reviewing and editing.

HIGHLIGHTS

- Two novel RC network models of active pipe-embedded structures (APES) are proposed
- The massiveness of APES systems impacts on the accuracy of simple RC network models
- A Genetic Algorithm is implemented to determine the RC network model parameters
- A Finite Difference in Frequency Domain model is used as the reference model
- The Umbrella RC network better predicts the thermal behavior of massive APES systems

Declaration of interests

☒ The authors declare that they have no known competing financial interests or personal relationships that could have appeared to influence the work reported in this paper.

☐The authors declare the following financial interests/personal relationships which may be considered as potential competing interests: